Dynamics of CO_2 fluxes and concentrations during a shallow subsurface CO_2 release

Jennifer L. Lewicki[1*], George E. Hilley[2], Laura Dobeck[3], and Lee Spangler[3]

[1*]Earth Sciences Division, Ernest Orlando Lawrence Berkeley National Laboratory, 1 Cyclotron Rd., Berkeley, CA, 94720 USA, e-mail: jllewicki@lbl.gov, ph: 510-495-2818, fax: 510-486-5686

[2]Department of Geological and Environmental Sciences, Stanford University, Stanford, CA, 94305 USA

[3]Department of Chemistry and Biochemistry, Montana State University, 108 Gaines Hall, PO Box 173400, Bozeman, MT, 59717 USA

Abstract. A field facility located in Bozeman, Montana provides the opportunity to test methods to detect, locate, and quantify potential CO_2 leakage from geologic storage sites. From 9 July to 7 August 2008, 0.3 t CO_2 d^{-1} were injected from a 100-m long, ~2.5 m deep horizontal well. Repeated measurements of soil CO_2 fluxes on a grid characterized the spatio-temporal evolution of the surface leakage signal and quantified the surface leakage rate. Infrared CO_2 concentration sensors installed in the soil at 30 cm depth at 0 to 10 m from the well and at 4 cm above the ground at 0 and 5 m from the well recorded surface breakthrough of CO_2 leakage and migration of CO_2 leakage through the soil. Temporal variations in CO_2 concentrations were correlated with atmospheric and soil temperature, wind speed, atmospheric pressure, rainfall, and CO_2 injection rate.

Keywords: Soil CO_2 flux; CO_2 concentration; Leakage; Geological carbon sequestration monitoring

1. Introduction

One approach being considered to help mitigate rising atmospheric CO_2 concentrations is geologic carbon sequestration (GCS), the storage in geological formations of CO_2 that is captured from industrial sources [e.g., International Energy Agency, 1997, 2004; IPCC, 2005]. While the purpose of GCS is to trap CO_2 underground, CO_2 could migrate away from the storage reservoir into the shallow subsurface and atmosphere if permeable pathways (such as well bores or faults) are present. A primary concern for the safety and effectiveness of GCS is therefore the possibility of leakage of CO_2 to the near-surface environment. Consequently, GCS requires monitoring techniques with the ability to detect, locate, and quantify potential CO_2 leakage in the near-surface environment.

Detection and characterization of potential CO_2 leakage will be challenging due to the large spatial and temporal variation in background CO_2 fluxes within which a leakage signal may exist (e.g., Lewicki et al., 2005; Cortis et al., 2008). To address this challenge, a facility was built in an agricultural field at Montana State University by the Zero Emissions Research and Technology (ZERT) Project to release CO_2 into the shallow subsurface from point and line sources. This facility provides the opportunity to test CO_2 measurement and modeling approaches and develop monitoring strategies for GCS sites. During summer 2007, two controlled releases of CO_2 were carried out over ten and eight days at different rates (0.1 and 0.3 t d^{-1}, respectively) from a shallow horizontal well. Based on repeated grid measurements of soil CO_2 flux, Lewicki et al. (2007) characterized the spatiotemporal evolution and quantified the surface leakage rates

of the signals associated with these relatively short releases. During summer 2008, CO_2 was released from the horizontal well over a one month period at 0.3 t d^{-1}. This experiment provided the chance to monitor the development of a CO_2 leakage signal associated with a release rate that was the same as in 2007, but over a comparatively longer time frame.

Building on the work of Lewicki et al. (2007), during summer 2008 we made repeated measurements of soil CO_2 flux on a grid surrounding the well, while continuously monitoring soil and atmospheric CO_2 concentrations [CO_2] and ancillary environmental parameters at several locations. Based on these measurements, we (1) characterize the spatiotemporal evolution of both CO_2 leakage and background biological (ecosystem respiration) fluxes, (2) quantify surface CO_2 leakage rates and their change over time, (3) characterize the development and decay of the leakage signal as expressed in atmospheric and soil [CO_2] at varying distances from the well, and (4) investigate relationships between temporal variations in CO_2 fluxes and concentrations and environmental parameters. Finally, we discuss implications of our observations for near-surface monitoring and modeling strategies at GCS sites.

2. Field Site and CO_2 Release Experiment

The CO_2 release experiment was carried out at Montana State University, at the Montana Agricultural Experiment Research Center in Bozeman, MT (45°39'N, 111°04'W). The study site was a ~0.12 km^2, nearly flat field, with vegetation composed primarily of

prairie grasses, alfalfa, and Canadian thistle. A ~0.2 to 1.2 m-thick clay topsoil here overlies an alluvial sandy cobble. A well, 100 m in length and oriented northeast-southwest, was installed in the field with a 70-m-long perforated and nearly-horizontal section at its center and unperforated sections on its two sloping ends (Figures 1a and 2). The perforated section was located at ~1.3-2.5 m depth, which was below the water table within the alluvial sandy cobble. This section was divided into six zones separated by 0.4-m wide inflatable packers. Five zones were 12 m in length and one zone (on the far southwest end of the well) was 9 m in length. When inflated, these packers prevented fluid flow between the six perforated well zones. From 9 July to 7 August 2008, 0.3 t CO_2 d^{-1} (300 kg CO_2 d^{-1}) were released from the well, approximately 39 kg d^{-1} from the perforated zone on the far southwest end of the well and 52 kg CO_2 d^{-1} from each of the other perforated zones. CO_2 flow rate to, and pressure within each of the perforated well zones were monitored during the release; however, due to recording difficulties, the longest continuous time series of these data was recorded from 23 July to 4 August 2008. The time series of CO_2 flow rate over this period is shown in Figure 3g for the Zone 5 injection zone (Figure 1a) and indicates that CO_2 injection unintentionally halted for about two hours on 25 July and about one hour on 26 July, the cause of which was unknown. For further details on the experiment design, the reader is referred to Spangler et al. (this issue).

3. Methods

A meteorological station was deployed 35 m northwest of the center of the well from 28 May to 4 September 2007 (Figure 2). Atmospheric pressure was measured using a Vaisala PTB101B barometer. Atmospheric temperature and relative humidity were measured using a Vaisala HMP50 humidity and temperature probe. Mean horizontal wind speed and direction were measured by a Gill-Solent WindMaster Pro sonic three-dimensional anemometer (Gill Instruments, Ltd) and a Climatronics CS800-12 wind set (Climatronics Corp.). Precipitation was measured by a TE525 tipping bucket rain gage (Texas Electronics). Soil moisture was measured at 30 cm depth at four locations within 5 m of the meteorological station using ECH2O (Decagon Devices) soil moisture probes. Since the soil moisture probes were neither calibrated for the soil at the study site nor corrected for diurnal variations in soil temperature, we refer to measurements as "relative soil moisture", and only assess the data qualitatively. Soil temperature was measured at 30 cm depth at two locations corresponding to the locations of two of the soil moisture probes with thermocouples. With the exception of wind speed and direction measured by the sonic anemometer at 10 Hz frequency, all variables were measured every 5 seconds and averaged over 30 minutes. Half-hour relative soil moistures were averaged for the four probes and half-hour soil temperatures were averaged for the two thermocouples.

Soil CO_2 flux was measured using a West Systems Fluxmeter (West Systems) based on the accumulation chamber method (e.g., Chiodini et al., 1998), with accuracy and repeatability of -12.5% (Evans et al., 2001) and ±10% (Chiodini et al., 1998), respectively. An opaque chamber was used and vegetation within the chamber footprint area was clipped so that only soil CO_2 efflux (ecosystem respiration + leakage) was

measured. Soil CO_2 flux was measured on a grid repeatedly on a daily basis at 10-m spacing from 6 to 8 July 2008 and repeatedly (on 13 days) at 2.5 to 10-m spacing from 9 July to 1 August 2008 (Figure 2). CO_2 flux was measured at 1-m spacing along the surface well trace on 8 July 2008 (Figure 1). On any given day, soil CO_2 fluxes were measured between 6:00 and 15:00. Maps of log soil CO_2 flux were interpolated based on grid measurements using a minimum curvature spline technique.

Soil [CO_2] was measured at 30 cm depth at 0, 2.5, 5, 7.5 and 10 m from the well (Figure 2) using Vaisala CARBOCAP® GMT221 non-dispersive infrared sensors (Vaisala, Inc.). These sensors (15.5 cm in length and 1.85 cm in diameter) were mounted within PVC tubes 25 cm in length and 2.5 cm in diameter. The top of each tube was sealed with a rubber stopper and the bottom was left open and buried at 30 cm depth in the soil. This design prevented contact of the sensors with liquid water, while allowing soil gas to diffuse to the sensor. The measurement range and accuracy were 0-20 vol.% (at standard temperature and pressure) and ±0.2 vol.% plus 2% of reading, respectively. Atmospheric [CO_2] was measured at 4 cm above the ground directly above the soil [CO_2] sensors located at 0 and 5 m from the well (Figure 2) using Vaisala CARBOCAP® GMT222 sensors. To protect from rain, these sensors were mounted within PVC tubes as described for soil [CO_2] sensors and installed above the ground. The measurement range and accuracy were 0-2000 ppmv (at standard temperature and pressure) and ±20 ppmv plus 2% of reading, respectively. Soil and atmospheric [CO_2] were measured every 1 second and averaged over 30 minutes. Half-hour [CO_2] measurements were corrected for

variations in pressure and temperature from the reference pressure and temperature of the sensors based on the ideal gas law.

4. Results

4.1 Environmental parameters

Times series of atmospheric and soil temperature, relative soil moisture content, half-hour cumulative precipitation, wind speed and atmospheric pressure are presented in Figure 3. All parameters (with the exception of cumulative precipitation) showed diurnal variations, superimposed on both longer-term and shorter-terms fluctuations. The heavy rain event occurring on 18 July was followed by a sudden increase in relative soil moisture content and decrease in soil temperature (Figure 3b-d). Relative soil moisture content showed a gradual long-term (multi-week) decline following this rain event (Figure 3d). The heavy rain event that occurred on 22 July was not associated with a discernable increase in soil moisture at the probe locations. Atmospheric temperatures were more highly variable than soil temperatures. Daily maximum soil temperatures at 30 cm depth occurred around midnight and lagged behind maximum atmospheric temperatures by about eight hours (Figure 3a and b). A relatively large drop in atmospheric pressure occurred from 9 to 10 July; the subsequent rise in pressure was accompanied by elevated wind speeds on 10 to 11 July (Figure 3e and f). A relatively large drop in atmospheric pressure occurred again from 15 to 22 August.

To further investigate relationships between environmental parameters on diurnal timescales, we isolated those variations by applying a 2nd order Butterworth band-pass filter (pass band at 0.9 to 1.1 cycles d^{-1}) to the signals. Correlation coefficients were then calculated as a function of time between pairs of parameters for a one-day moving window (half-hour time step) through the time series. Results are shown in Figure 4. Atmospheric temperature was moderately to well negatively correlated (correlation coefficients ~-0.5 to -0.9) with soil temperature and atmospheric pressure over the observation period (Figure 4a and b), whereas it was positively correlated with wind speed around 10 July, and then negatively correlated with wind speed for much of the rest of the measurement period (Figure 4b).

Atmospheric pressure and wind speed showed a peak in positive correlation around 10 July (Figure 4d). With the exception of a drop to negative correlation around 17 August, these parameters were moderately to well positively correlated (correlation coefficients ~0.5 to 1.0) from about 18 July until the end of the measurement period. With the exception of around 10 July when soil temperature and wind speed were well negatively correlated, these parameters were typically poorly to well positively correlated (Figure 4e). Soil temperature and atmospheric pressure were typically poorly correlated (correlation coefficients ~-0.3 to 0.3) over the observation time (Figure 4f).

4.2 Soil CO_2 fluxes

Grid measurements of soil CO_2 flux mapped background soil respiration fluxes prior to, and the spatio-temporal evolution of the surface CO_2 flux leakage signal during the CO_2 release (Figure 5). Following the methods of Lewicki et al. (2007), we estimated total CO_2 discharge (D_{tot}, t CO_2 d^{-1}) for each grid dataset by calculating the declustered mean CO_2 flux using GSLIB (Deutsch and Journel, 1998) and multiplying it by the grid area (7700 m^2). D_{tot} therefore includes CO_2 discharge associated with background processes (i.e., ecosystem respiration) plus CO_2 leakage. Background CO_2 discharge (D_{back}) was equal to D_{tot} from 6 to 9 July. After the release began, we did not observe evidence of surface CO_2 leakage at distances greater than 7.5 m from the well trace. We therefore estimated D_{back} for each grid dataset after 9 July by multiplying the average of CO_2 fluxes measured at distances ≥10 m from the well trace by 7700 m^2. Leakage CO_2 discharge (D_{leak}) was then estimated for each grid dataset by subtracting D_{back} from D_{tot}. D_{tot}, D_{back}, and D_{leak} are plotted on Figure 3h as a function of time.

Background soil CO_2 fluxes were measured repeatedly on the grid from 6 to 9 July 2008 and, on average (D_{back} = 0.12 to 0.16 t d^{-1}), were similar over that period (Figures 3h and 5a-d). Since the CO_2 release began at approximately 16:00 on 9 July 2008, after soil CO_2 flux measurements were completed on that day, measurements on 9 July are regarded as background values. Breakthrough of CO_2 leakage at the surface was observed at six point sources aligned along the well trace on 10 July after less than one day of CO_2 injection (Figure 5e). The D_{leak} estimated on 10 July was 0.26 t d^{-1} (Figure 3h). The magnitude of the surface CO_2 leakage signal then increased (to D_{leak} = 0.34 t d^{-1}) over the next three days, reaching near-steady state on 13 July, while D_{back} remained

relatively constant (Figure 3h). Some spreading of leaking CO_2 was observed both along and away from the well trace during this time; the spatial distribution of the leakage signal then remained relatively constant throughout the rest of the observation period. Following a gap in soil CO_2 flux measurements from 16-22 July, D_{leak} showed a large degree of variability (0.24 to 0.44 t d^{-1}) from 22 to 30 July, and then remained constant at around 0.32 t d^{-1} on 1-2 August (Figure 3h). D_{back} increased between 15 and 22 July and between 22 and 23 July, and then remained relatively stable over rest of the measurement period.

Figure 1 elucidates the spatial relationship between soil CO_2 fluxes measured on 14 July at one-m spacing along the surface well trace and the design of the horizontal well. Peaks in CO_2 leakage fluxes were observed above the inflatable packers on the relatively high elevation ends of five of the perforated injection zones.

4.3 Atmospheric and soil [CO_2]

Time series of atmospheric and soil [CO_2] are presented in Figure 6. Prior to the start of the CO_2 release, atmospheric and soil [CO_2] showed diurnal fluctuations, with relatively high atmospheric values observed during the nighttime and relatively high soil values observed during the daytime, typically in late afternoon. The means and standard deviations of the 0 and 5 m atmospheric [CO_2] measurements were 462 ± 80 and 478 ± 69 ppmv, respectively. Mean soil [CO_2] values measured prior to the release at 0 to 10 m

from the well ranged from 0.6 to 1.0 vol.%; the standard deviation for all sensors was 0.1 vol.%.

Anomalously high (>1000 ppmv) atmospheric [CO_2] were measured ~5 and 9 hours after the release start at the 0 and 5 m sensors, respectively (Figure 6a and b), and prior to the observation of elevated soil [CO_2] values at the corresponding soil sensors located 0 and 5 m from the well (Figure 6c). As observed before the release, relatively high and low atmospheric [CO_2] tended to be observed during the nighttime and daytime, respectively. However, the means and standard deviations of atmospheric [CO_2] measured during the release at the 0 and 5 m sensors increased to 881 ± 379 and 702 ± 273 ppmv, respectively. Atmospheric [CO_2] values measured at the 0 m sensor exceeding its measurement range (indicated by [CO_2] > 2500 ppmv on Figure 6a) were not included in calculations of mean and standard deviation; these parameters are therefore regarded as underestimates. Mean daily atmospheric [CO_2] measured at 0 m from the well dropped suddenly at the end of the release, followed by a more gradual decline over the following ~15 days to values similar to those measured prior to the release (Figure 5a). In contrast, mean daily atmospheric [CO_2] at the 5 m sensor increased over about three days following the end of the release, and then gradually declined over the remainder of the observation period (Figure 5b). At the end of the observation period, atmospheric [CO_2] values at 5 m from the well remained higher on average than those measured prior to the release.

Soil [CO_2] measured by the 0, 2.5, and 5 m sensors displayed exponential increases and decreases following the beginning and end of the CO_2 release, respectively (Figure 6c). The increases began about one, two, and seven days after the start of the release at the 0, 2.5, and 5 m sensors, respectively. Soil [CO_2] measured 0, 2.5, and 5 m from the well reached maximum values of 14.0, 11.5, and 4.0 vol.%, respectively. Diurnal and higher-frequency fluctuations in [CO_2] were superimposed on the long-term variation in soil [CO_2] at these sensors related to the CO_2 injection. For example, soil [CO_2] suddenly dropped by up to ~ 7 vol.% and then recovered at the 0 m sensor on 20, 25, and 26 July and 5 and 7 August, where the drop on 7 August corresponded to the end of the release. These drops were temporally correlated with sudden increases, then drops in soil [CO_2] at the 2.5 m sensor. On July 25 and 26, they were also temporally correlated with drops in soil [CO_2] at 5 m from the well and atmospheric [CO_2] at 0 and 5 m from the well (Figure 6). After soil [CO_2] recovered at the 0 m sensor at the end of the release, it remained relatively high for about one day, and then declined exponentially over the remainder of the observation period to near values measured prior to the release. The decline in soil [CO_2] at the 2.5 m sensor began immediately after the release end and continued to near values measured before the start of the release. Similar to trends observed in atmospheric [CO_2] at the 5 m sensor, soil [CO_2] measured 5 m from the well increased over about three days after the end of the release, and then gradually decreased over the remainder of the measurement period. These values remained elevated on average relative to those measured before the release. Soil [CO_2] measured at sensors located 7.5 and 10 m from the well displayed a gradual increase up to about 2 vol.% from 18 to 26 July, and then a

long-term decline over the remainder of the measurement period to values similar to those observed before the release start.

Soil and atmospheric [CO_2] measured at all distances from the well displayed fluctuations over long-term (multi-day to multi-week), moderate (diurnal), and short-term (less than one day) timescales (Figure 6). The long-term elevated [CO_2] signals observed at the 0, 2.5, and 5 m sensors were coincident with, with varying time lags behind, the CO_2 release. At the 5, 7.5 and 10 m sensors, soil [CO_2] showed some general correlations with rain events and changes in relative soil moisture (Figure 3c and d). For example, soil [CO_2] at these sensors displayed sudden increases following the heavy rain events on 18 and 22 July, which then persisted for several days. Soil [CO_2] at the 7.5 and 10 m sensors then showed long-term declines that generally corresponded to the decline in relative soil moisture over the rest of the measurement period. Irregular, high-frequency drops in atmospheric and soil [CO_2] at the 0, 2.5, and 5 m sensors on 25 and 26 July were coincident with the unintended loss of CO_2 flow to the well (Figure 3g).

To further investigate relationships between diurnal variations in atmospheric and soil [CO_2] and environmental parameters, we isolated diurnal variations in [CO_2] by applying a 2nd order Butterworth band-pass filter (pass band at 0.9 to 1.1 cycles d^{-1}) to the signals as described above for environmental parameters. Figures 7-9 show correlation coefficients plotted as a function of time for a one-day moving window (half-hour time step) through the time series of atmospheric [CO_2] measured at 5 m from the well and soil [CO_2] measured at 0, 2.5, 5, and 10 m from the well versus environmental

parameters. Results are not shown for atmospheric [CO_2] at the 0 m sensor due to loss of data when the sensor measurements were off scale. Also, correlations over time between soil [CO_2] measured at 7.5 m from the well and environmental parameters were similar to those in Figure 10 for soil [CO_2] measured at the 10 m sensor and are therefore not presented.

Atmospheric [CO_2] measured 5 m from the well was well inversely correlated (correlation coefficients ~-0.9 to -1.0) with atmospheric temperature for the entire observation period (Figure 7a). Atmospheric [CO_2] and wind speed were moderately to strongly positively correlated (correlation coefficients ~0.5 to 1.0) over the observation time, except around 10 July when they became well negatively correlated (correlation coefficients ~-1.0; Figure 7b). Atmospheric [CO_2] and pressure showed poor to moderate positive correlation (correlation coefficients ~0.0 to 0.5) over much of the observation period (Figure 7c).

Soil [CO_2] at the 0 m sensor was more consistently negatively correlated with soil temperature (Figure 8a), whereas at the 2.5 to 10 m sensors, it was more consistently positively correlated with soil temperature (Figures 8a and 9a). Correlations between wind speed and soil [CO_2] at all sensors dropped sharply toward negative values on 10 July, and then rose to positive values (Figures 8b and e and 9b and e). Correlations between wind speed and soil [CO_2] over the rest of the measurement time were more consistently negative at the 0 m sensor, highly variable at the 2.5 m sensor, and more consistently positive at the 5 and 10 m sensors. Similarly, correlations between

atmospheric pressure and soil [CO_2] were more commonly negative at the 0 m sensor, highly variable at the 2.5 m sensor, and more commonly positive at the 5 m sensor, whereas at the 10 m sensor this relationship was highly variable (Figures 8c and f and 9c and f). For a given soil [CO_2] sensor, changes in the sign of the correlation often occurred concurrently between [CO_2] and different environmental parameters. For example, at the 0 m sensor, the correlations between [CO_2] and soil temperature, wind speed, and atmospheric pressure all shifted upwards toward positive values around 23 July and 17 August (Figure 8a-c). At the 2.5 m sensor, correlations between [CO_2] and soil temperature and wind speed shifted to negative values and correlation between [CO_2] and atmospheric pressure shifted to positive values around 23 July and 17 August (Figure 8d-f). Finally, downward shifts in correlations toward negative values were observed between soil [CO_2] and all three environmental parameters around 28 July at the 5 m sensor (Figure 9a-c).

As introduced above, anomalously high [CO_2] was measured at the 0 and 5 m atmospheric sensors before it was measured at the corresponding 0 and 5 m soil sensors below. In Figure 10, we examine the relationship between atmospheric [CO_2] and wind speed and direction from 10 to 17 July, the time frame between the appearance of elevated atmospheric [CO_2] and that of elevated soil [CO_2] at the 5 m sensors. Assuming atmospheric [CO_2] values > 1000 ppmv were anomalously high, 88% of anomalously high values were measured when average half-hour winds were westerly to southerly (150 to 300°), with speeds from about 1.5 to 6 m s^{-1} (Figure 10), in other words, when the

sensor was located downwind of the two surface leakage point sources on the far southwest end of the well (Figure 5).

5. Discussion and Conclusions

Our measurements of soil CO_2 fluxes and atmospheric and soil [CO_2] recorded the development and decay in both space and time of the near-surface leakage signal associated with a controlled CO_2 release. As indicated by atmospheric [CO_2] measurements, breakthrough of CO_2 leakage at the surface occurred quickly ($\leq$ 5 hours after the start of the release; Figure 6a). Soil CO_2 fluxes measured on the grid and at one-m spacing along the surface trace of the well showed that the surface leakage signal was expressed as five to six point sources aligned along the well (Figures 1 and 5). These areas of focused CO_2 emission were typically observed above the relatively high elevation ends of well injection zones and above and only slightly offset from packer locations (Figure 1). Based on these observations, it is likely that CO_2 migrated from relatively low to high elevation within injection zones until it encountered the barriers of the packers (e.g., Lewicki et al., 2007). It probably then migrated vertically and relatively rapidly to the surface along high permeability pathways in the cobble and soil layers.

Atmospheric [CO_2] sensors at 0 and 5 m from the well detected surface breakthrough of leakage before it was detected by soil [CO_2] sensors located directly below them and by daily grid measurements of soil CO_2 flux. Also, prior to detection of anomalously high

[CO_2] at the 5 m soil sensor, anomalously high [CO_2] was measured at the 5 m atmospheric sensor typically when winds were blowing from the direction of the well (Figure 10). These observations suggest that injected CO_2 traveled relatively quickly along high-permeability pathways to reach the surface initially at locations away from the 0 and 5 m atmospheric [CO_2] sensors. It was likely then transported in the atmosphere to the sensors. Our atmospheric [CO_2] sensors probably detected the leakage signal clearly because they were located near the ground surface and the well, thus minimizing dilution of the leakage signal with atmospheric air. Therefore, if sensors are strategically placed relative to the locations of most-likely leakage sources, atmospheric [CO_2] measurements may be a useful tool to detect arrival of CO_2 leakage at the surface.

Based on soil CO_2 flux measurements, we estimated D_{leak} and its change over time (Figure 3h). Over the observation period following the release start (10 July to 2 August), the mean and standard deviation of D_{leak} were 0.31 and 0.05 t d^{-1}, respectively. This suggests that most CO_2 injected into the well was emitted at the surface (i.e., minimal CO_2 was dissolved in the groundwater system). The variability in D_{leak} from 22 to 30 July could have been due in part to changes in soil physical properties associated with the heavy rain events that occurred on 18 and 22 July. However, more detailed characterization of spatial and temporal variations in soil CO_2 fluxes and soil physical properties are required to resolve these relationships. Our results overall indicate that the accumulation chamber method is a reliable technique to detect, characterize the spatial distribution of, and quantify surface CO_2 flux leakage signals similar to that produced in this experiment.

Continuous measurements of soil [CO_2] recorded at high temporal resolution the development and decay of the CO_2 signal associated with one of the leakage point sources along the well (Figure 6c). The leakage signal, expressed as elevated soil [CO_2] over multiple weeks, was clearly detected at sensors located 0, 2.5, and 5 m from the well, which was consistent with soil CO_2 flux measurements (Figure 5). The leakage signal dominated the long-term (multi-week) variation in [CO_2] at these sensors. Also, the start and end of the CO_2 release were followed by exponential increases and decreases, respectively, in soil [CO_2] at the 0-5 m sensors after the start and end, respectively, of the CO_2 release; inversion of these exponential curves using, for example, a flow and transport simulator could constrain a conceptual model of the shallow subsurface and transport processes. Several irregular, high-frequency drops in soil [CO_2] occurred at the 0-5 m sensors during the CO_2 release and were likely caused by unintended loss of CO_2 flow to the well (Figures 3g and 6c). Long-term (multi-week) variations in soil [CO_2] at sensors located 7.5 and 10 m from the well were subtle relative to those observed at the 0-5 m sensors (Figure 6c). It was therefore difficult to detect a potential component of leakage-derived CO_2 at the 7.5 and 10 m sensors; soil CO_2 here was likely predominantly of background (e.g., ecosystem respiration) origin. Carbon isotopic measurements at these sensors would be valuable to detect potential contribution of injected CO_2.

Variations in background environmental parameters can strongly modulate changes in soil and atmospheric [CO_2]. We investigated qualitative relationships between

environmental parameters and soil and atmospheric [CO_2] on diurnal timescales by applying a band pass filter to the time series to isolate diurnal variations, followed by simple correlation analysis. The strong negative correlation observed over the entire observation period between atmospheric [CO_2] measured 5 m from the well and atmospheric temperature (Figure 7a) reflects plant photosynthetic uptake of atmospheric CO_2 during the daytime when temperature is relatively high and ecosystem respiration when temperature is relatively low. We might expect to observe a negative correlation between wind speed and atmospheric [CO_2] due to increased atmospheric mixing with increased wind speed. However, with the exception of the inverse correlation observed during the period of high winds on 10 to 11 July, atmospheric [CO_2] and wind speed were typically positively correlated (Figure 7b). The inverse correlation observed between wind speed and atmospheric temperature over much of the observation period (Figure 4b) complicates interpretations of the influence of wind speed on atmospheric [CO_2].

Relationships between soil [CO_2] and environmental parameters on diurnal timescales varied widely between sensors at different distances from the well, as well as over time at individual sensors (Figures 8 and 9). The strength and sense (positive or negative) of these correlations were probably controlled by a range of factors, such as (1) soil physical properties (e.g., air-filled porosity and permeability), (2) the origin of soil CO_2 (e.g., ecosystem respiration versus injection-derived), (3) the dominant transport mechanism of soil CO_2, concentration gradient-driven (diffusive) versus pressure gradient-driven (advective), (4) the relative strength of the forcing of the environmental parameters, and

(5) cross-correlations between environmental variables themselves. The first four factors are largely unknown at our study site. Also, if two (or more) environmental parameters strongly co-vary, it is impossible to attribute changes in soil [CO_2] to an individual environmental parameter. Given these challenges, we only assess general relationships between soil [CO_2] and environmental variables and make a few broad suggestions regarding the physical mechanisms by which environmental variables may influence diurnal variations observed in soil [CO_2].

Soil temperature is a strong driver of ecosystem respiration on diurnal timescales (e.g., Smith et al., 2003 and references therein). Therefore, in the case where the source of soil CO_2 is derived in large part from respiration, we would expect positive correlation between soil [CO_2] and temperature, as observed at sensors located 7.5 and 10 m from the well (e.g., Figure 9d). Conversely, the highly variable and often negative correlation between soil [CO_2] and temperature at the 0 m sensor (Figure 8a) is likely associated with a large non-respiration-derived component of CO_2 here. The positive correlation observed between soil [CO_2] at 2.5 and 5 m sensors and soil temperature during portions of the observation period (Figures 8d and 9d) could reflect contribution of respiration-derived CO_2 and/or result from the positive correlation between wind speed and soil temperature at similar times (Figure 4e).

Variations in wind and atmospheric pressure can induce advective flow of soil gas (e.g., Clements and Wilkening, 1974; Nilson et al., 1991; Massmann and Farrier, 1992; Lewicki et al., 2003; Takle et al., 2004; Poulsen and Møldrup, 2006). For example,

wind-driven airflow over a rough surface can cause pressure differentials associated with drag. Advective flow of air into and out of a permeable soil should occur where pressure builds up and drops, respectively, at the soil surface. Infiltration of atmospheric air into the soil may lead to a decrease in soil [CO_2]. Whether positive or inverse correlation is observed at a given location between wind speed and soil [CO_2] will depend on a number of factors such as wind speed and direction, soil physical properties, and surface roughness. Diurnal variations in atmospheric pressure associated with thermal (heating and cooling of the atmosphere) and gravitational (earth-tide) effects can also drive advective airflow through permeable soil. Diurnal variations in atmospheric pressure may therefore be inversely correlated with changes in soil [CO_2].

Since we observed a positive correlation between atmospheric pressure and wind speed over much of the observation period (Figure 4d), it is difficult to discern the relative impacts of these parameters on soil [CO_2] variations. The negative correlations observed between wind speed and soil [CO_2] at all sensors and atmospheric pressure and soil [CO_2] at the 0-5 m sensors during the period of high winds and rising atmospheric pressure on 10 to 11 July (Figures 8 and 9) likely reflected enhanced flow of atmospheric air through soils. Over the rest of the observation period, strong inverse correlations were observed between soil [CO_2] and atmospheric pressure and wind speed more consistently at the 0 m sensor, relative to the 2.5-10 m sensors, where weaker correlations or strong positive correlations were observed more consistently between these parameters. Disparities in correlations observed at different sensors may be due in part to differences in soil gas transport mechanisms resulting from, for example, varying soil CO_2 flow rates, soil

physical properties, and/or surface roughness with distance from the well. Also, changes in the sense of the correlation (e.g., negative to positive) between soil [CO_2] at a given sensor and wind speed or atmospheric pressure over time could be related in part to variations in the relative strength of the meteorological forcing at the surface and the associated time required for soil [CO_2] to respond to the forcing at 30 cm depth. For example, as wind speeds decreased following the period of high winds on 10 to 11 July (Figure 3e), correlations between soil [CO_2] and wind speed changed from negative to positive at all sensors (Figures 8 and 9). High wind speeds (coupled with rising atmospheric pressure) likely caused relatively large perturbations in surface pressures, and therefore relatively rapid responses (decreases) in soil [CO_2] at depth, yielding the observed inverse correlations on 10 to 11 July. Weaker diurnal variations in wind speeds during the following days could have still produced decreases in soil [CO_2], but at a longer time lag behind increases in wind speed. Since we only calculated correlation coefficients for the case of no time lag between parameters, a decrease in soil [CO_2] hours after increase in wind speed may appear as a positive correlation between the two variables. Overall, detailed characterization of heterogeneities in soil physical properties, surface roughness, and contribution of injection-related to total CO_2 flow coupled with flow and transport modeling is required to better understand relationships between soil [CO_2] at different sensors and wind and atmospheric pressure.

Increases in soil moisture content associated with periodic precipitation events can lead to increase in soil [CO_2] due to elevated ecosystem respiration rates and/or decrease in soil air-filled porosity and permeability (suppressed CO_2 efflux from the soil). Subtle

increases in soil [CO_2] observed at the 5-10 m sensors (Figure 6c) following heavy precipitation events on 18 and 22 July (Figure 3c) may have been caused by modest increases in ecosystem respiration rates, as suggested by the increase in D_{back} over this timeframe (Figure 3h). Also, the subsequent long-term (multi-week) decline in soil [CO_2] at the 7.5 and 10 m sensors may have been related to a decrease in ecosystem respiration rates as soil dried out (Figures 3d and 6c).

Overall, our results indicate that point-measurement approaches of soil CO_2 fluxes and soil and atmospheric [CO_2] are promising tools for the detection, location, and quantification of near-surface CO_2 leakage signals. However, results presented here and by Lewicki et al. (2007) specifically pertained to the case where the location of the CO_2 leakage source was known a priori. Potential pathways for CO_2 leakage at GCS sites will likely be poorly constrained and located within large, reservoir-scale areas. Therefore, CO_2 point-measurement approaches should ideally be coupled with line and area-integrated CO_2 measurement (e.g., Humphries et al., 2008; Lewicki et al., in review) and remote sensing techniques (e.g., Male et al., this issue), as well as with statistical sampling and analysis approaches (e.g., Lewicki et al., 2005) to enhance their application in GCS monitoring programs.

Acknowledgements. We thank K.Gullickson for helpful assistance in the field. This work was funded by the ZERT Project, Assistant Secretary for Fossil Energy, Office of Sequestration, Hydrogen, and Clean Coal Fuels, NETL, of the U.S. Dept. of Energy under Contract No. DE-AC02-05CH11231.

References

Chiodini C, Cioni GR, Guidi M, Raco B, Marini L (1998) Soil CO_2 flux measurements in volcanic and geothermal areas. Appl Geochem 13: 543-552

Clements WE, Wilkening MH (1974) Atmospheric pressure effects on Rn^{222} transport across the earth–air interface. J Geophys Res 79: 5025–5029

Cortis A, Oldenburg, CM, Benson, SM (2008) The role of optimality in characterizing CO_2 seepage from geologic carbon sequestration sites. Int J Greenhouse Gas Control 2: 640–652

Evans WC, Sorey, ML, Kennedy BM, Stonestrom DA Rogie JD, Shuster DL (2001) High CO_2 emissions through porous media: Transport mechanisms and implications for flux measurement and fractionation. Chem Geol 177:15-29

Humphries SD, Nehrir AR, Keith CJ, Repasky KS, Dobeck L, Carlsten L, Spangler L (2008) Testing carbon sequestration site monitoring instruments using a controlled carbon dioxide release facility. Appl Optics 47: 548-555

International Energy Agency (1997) Carbon Dioxide Utilization. IEA Greenhouse Gas R and D Programme, Paris

International Energy Agency (2004) Prospects for CO_2 Capture and Storage. IEA Publications, Paris

IPCC (2005) IPCC Special Report on Carbon Dioxide Capture and Storage. Cambridge University Press, Cambridge

Lewicki JL, Evans WC, Hilley GE, Sorey ML, Rogie JD, Brantley SL (2003) Shallow soil CO_2 flow along the San Andreas and Calaveras faults, California. J Geophys Res 108: 2187 doi:101029/2002JB002141

Lewicki JL, Hilley GE, Oldenburg CM (2005) An improved strategy to detect CO_2 leakage for verification of geologic carbon sequestration. Geophys Res Lett 32: L19403 doi:10.1029/2005GL024281

Lewicki JL, Oldenburg CM, Dobeck L, Spangler L (2007) CO_2 leakage during two shallow subsurface CO_2 releases. Geophys Res Lett 34: L24402 doi:10.1029/2007GL032047

Lewicki JL, Hilley GE, Fischer ML, Pan L, Oldenburg CM, Dobeck L, and Spangler L (in review) Eddy covariance observations of surface CO_2 leakage during shallow subsurface CO_2 releases. J Geophys Res

Male EJ, Pickles WL, Silver EA, Hoffmann G, Lewicki JL, Apple M, Repasky K, Burton EA (this issue) Using hyperspectral plant signatures for CO_2 leak detection during the 2008 ZERT CO_2 sequestration field experiment in Bozeman, MT. Env Earth Sciences

Massmann J, Farrier DF (1992) Effects of atmospheric pressures on gas transport in the vadose zone. Water Resources Res 28: 777–791

Nilson RH, Peterson EW, Lie KH, Burkhard NR, Hears JR (1991) Atmospheric pumping: a mechanism causing vertical transport of contaminated gases through fractured permeable media. J Geophys Res 96: 21933–21948

Poulsen T, Møldrup P (2006) Evaluating effects of wind-induced pressure fluctuations on soil-atmosphere gas exchange at a landfill using stochastic modelling. Waste manage Res 24: 473-481

Smith KA, Ball T, Conen F, Dobbie KE, Massheder J, Rey A (2003) Exchange of greenhouse gases between soil and atmosphere: interactions of soil physical factors and biological processes. Eur J Soil Sci 54: 779-791

Spangler LH, Dobeck LM, Repasky K, et al. (this issue) A controlled field pilot in Bozeman, Montana, USA, for testing near surface CO_2 detection techniques and transport models. Env Earth Sciences

Takle ES, Massman WJ, Brandlec JR, Schmidt RA, Zhou X, Litvina IV, Garcia R, Doyle G, Rice CW (2004) Influence of high-frequency ambient pressure pumping on carbon dioxide efflux from soil. Agri Forest Met 124: 193-206

Figure Captions

Figure 1. (a) Elevations of ground surface, water table, and horizontal well versus distance along well. Location of injection zone 5 is shown. (b) Soil CO_2 flux measured along the surface trace of the horizontal well on 14 July 2008.

Figure 2. Schematic showing locations of meteorological station (star), soil CO_2 flux measurements on grid (circles), and [CO_2] sensors (squares), relative to surface trace of the horizontal well (black line). White squares indicate locations of atmospheric and soil [CO_2] sensors at 0 and 5 m from the well and black squares indicate locations of soil [CO_2] sensors at 2.5, 7.5, and 10 m from well.

Figure 3. Time series of (a) atmospheric temperature, (b) soil temperature (30 cm depth), (c) half-hour cumulative precipitation, (d) relative soil moisture (30 cm depth), (e) wind speed, (f) atmospheric pressure, (g) and CO_2 flow (injection) rate recorded from 23 July to 4 August 2008 in zone 5 of the well. (h) Plot of CO_2 discharge versus time estimated based on soil CO_2 flux measurements on grid. Dots, circles, and diamonds are total (D_{tot}), background (D_{back}), and leakage (D_{leak}) CO_2 discharge, respectively.

Figure 4. Correlation coefficient as a function of time for atmospheric temperature versus (a) soil temperature, (b) wind speed, and (c) atmospheric pressure and for (d) wind speed versus atmospheric pressure, (e) soil temperature versus wind speed, and (f) soil

temperature versus atmospheric pressure. Dashed lines show start and end of the CO_2 release.

Figure 5. Maps of log soil CO_2 flux interpolated based on measurements made at the black dots. White line and squares on (a) show locations of surface trace of well and [CO_2] sensors, respectively (Figure 2).

Figure 6. Time series of (a) atmospheric [CO_2] measured at 4 cm height and 0 m from the well (values above 2500 ppmv are off scale), (b) atmospheric [CO_2] measured at 4 cm height and 5 m from the well, and (c) soil [CO_2] measured at 30 cm depth and 0 (black dots), 2.5 (red dots), 5 (blue dots), 7.5 (green dots), and 10 (magenta dots) m from the well. Dashed lines show start and end of the CO_2 release.

Figure 7. Correlation coefficient as a function of time for atmospheric [CO_2] measured 5 m from well versus (a) atmospheric temperature, (b) wind speed, (c) atmospheric pressure, and (d) soil [CO_2] measured 5 m from well. Dashed lines show start and end of the CO_2 release.

Figure 8. Correlation coefficient as a function of time for soil [CO_2] measured 0 m from well versus (a) soil temperature, (b) wind speed, and (c) atmospheric pressure and for soil [CO_2] measured 2.5 m from well versus (d) soil temperature, (e) wind speed, and (f) atmospheric pressure. Dashed lines show start and end of the CO_2 release.

Figure 9. Correlation coefficient as a function of time for soil [CO_2] measured 5 m from well versus (a) soil temperature, (b) wind speed, and (c) atmospheric pressure and for soil [CO_2] measured 10 m from well versus (d) soil temperature, (e) wind speed, and (f) atmospheric pressure. Dashed lines show start and end of the CO_2 release.

Figure 10. Radial plot of log atmospheric [CO_2] measured 10-17 July 2008, 5 m from the well as a function of wind speed and direction. Color bar denotes [CO_2].

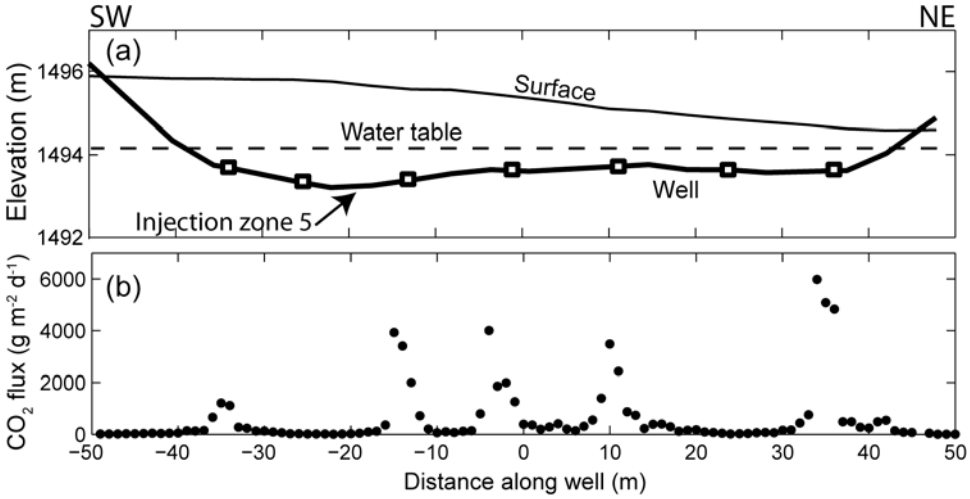

Figure 1.

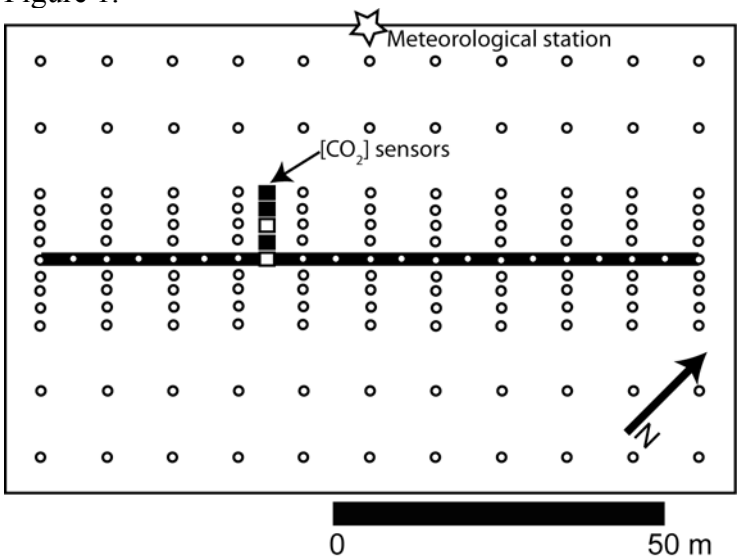

Figure 2.

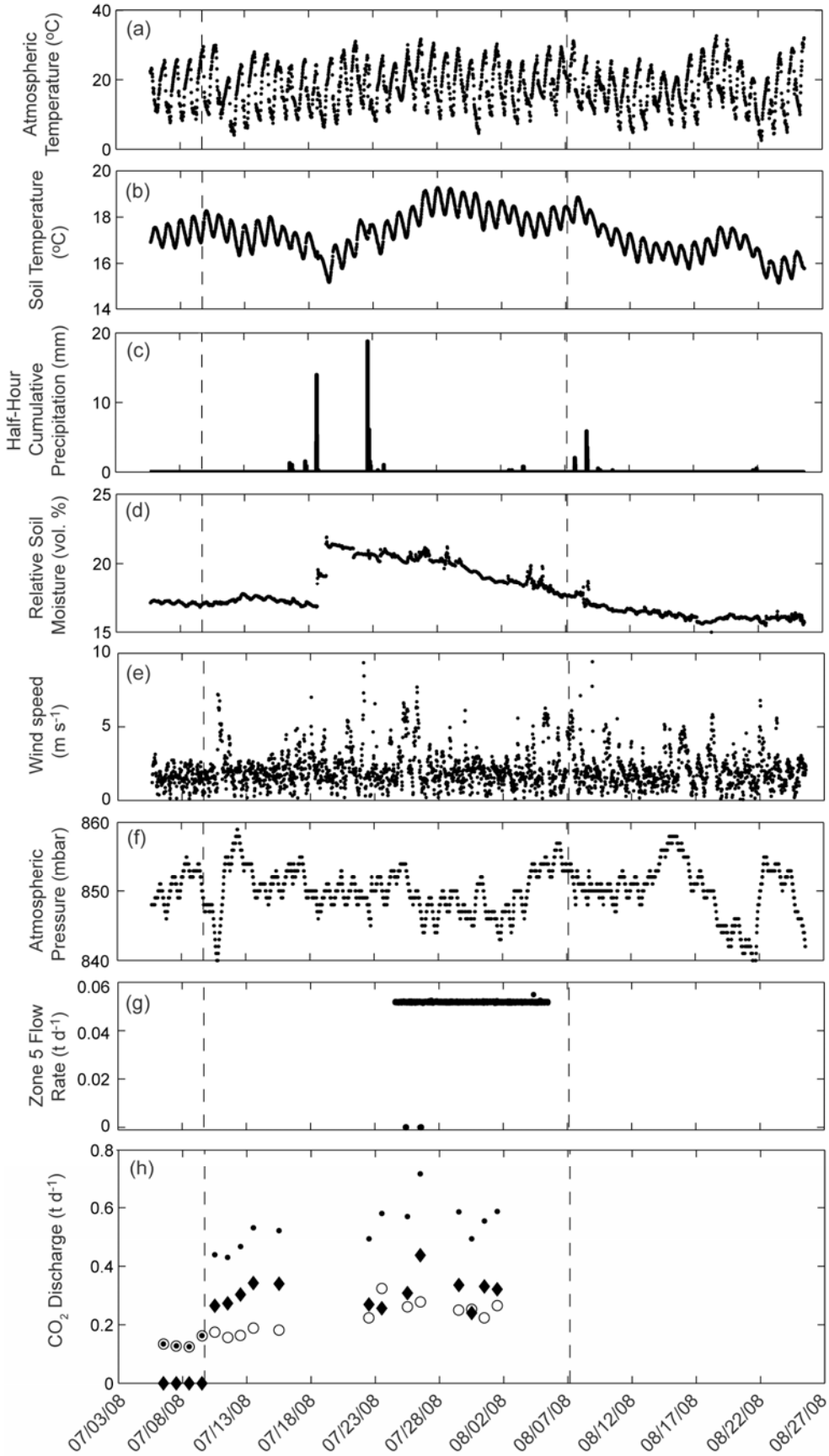
(a)
Atmospheric Temperature (°C)
(b)
Soil Temperature (°C)
(c)
Half-Hour Cumulative Precipitation (mm)
(d)
Relative Soil Moisture (vol. %)
(e)
Wind speed (m s-1)
(f)
Atmospheric Pressure (mbar)
(g)
Zone 5 Flow Rate (t d-1)
(h)
CO2 Discharge (t d-1)
07/03/08
07/08/08
07/13/08
07/18/08
07/23/08
07/28/08
08/02/08
08/07/08
08/12/08
08/17/08
08/22/08
08/27/08

Figure 3.

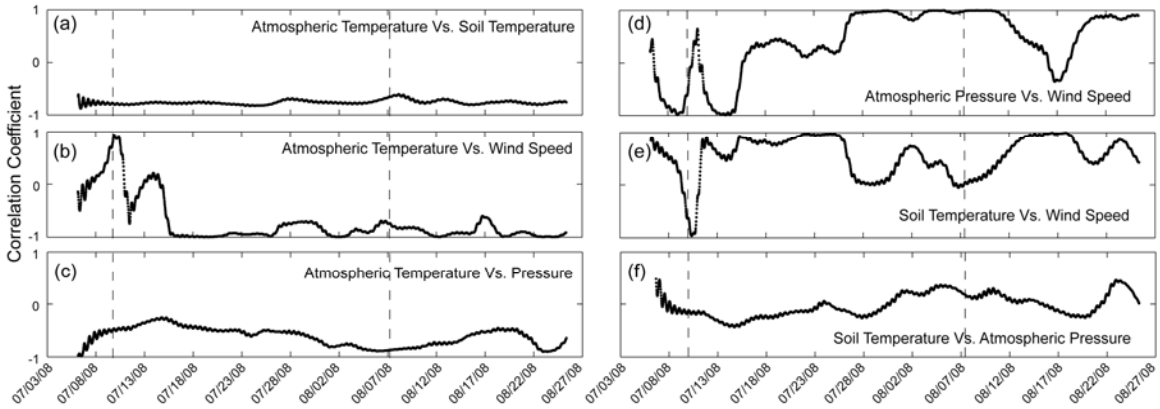

Figure 4.

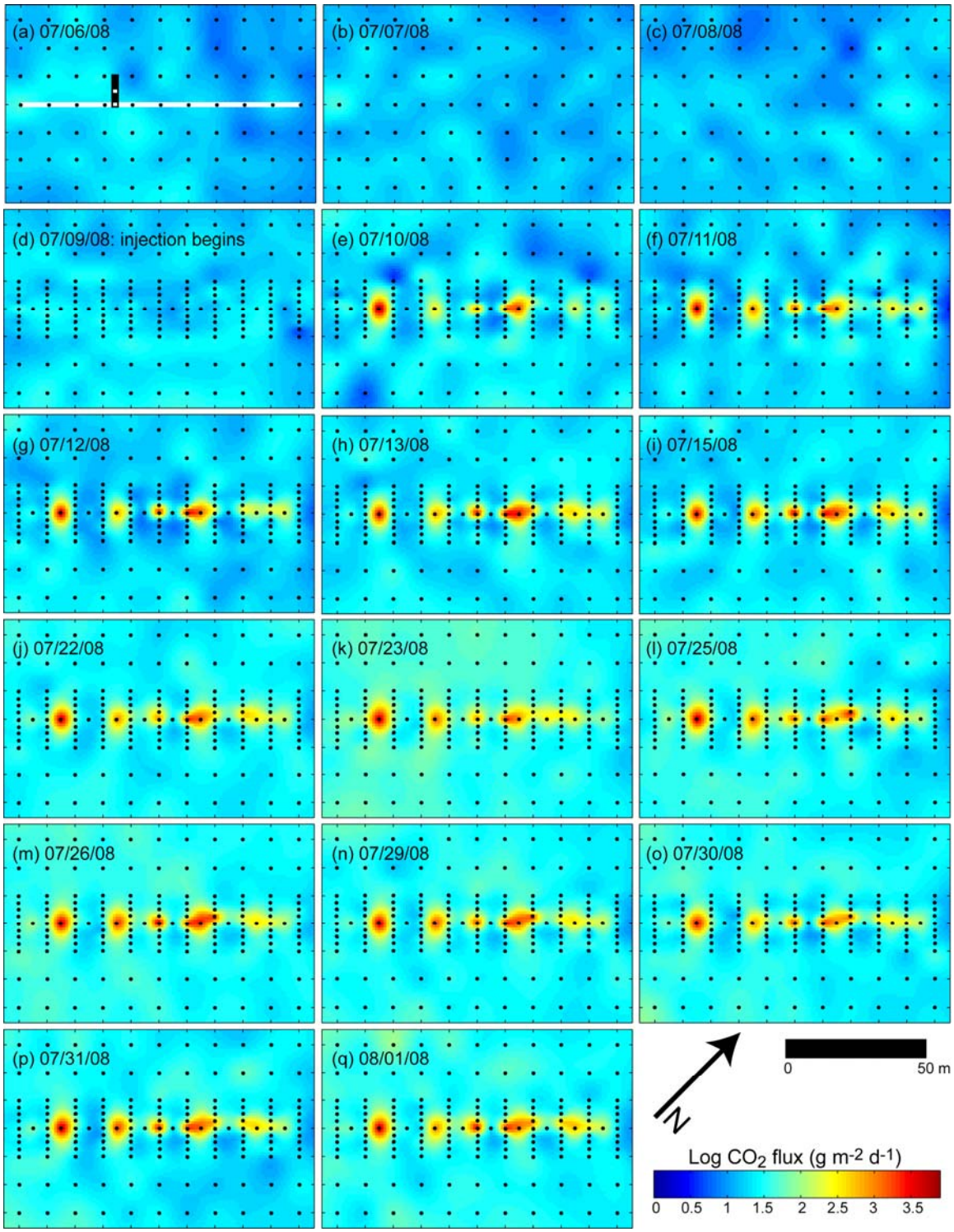
(a) 07/06/08
(b) 07/07/08
(c) 07/08/08
(d) 07/09/08: injection begins
(e) 07/10/08
(f) 07/11/08
(g) 07/12/08
(h) 07/13/08
(i) 07/15/08
(j) 07/22/08
(k) 07/23/08
(l) 07/25/08
(m) 07/26/08
(n) 07/29/08
(o) 07/30/08
(p) 07/31/08
(q) 08/01/08
0
50 m
N
Log CO2 flux (g m-2 d-1)
0 0.5 1 1.5 2 2.5 3 3.5

Figure 5.

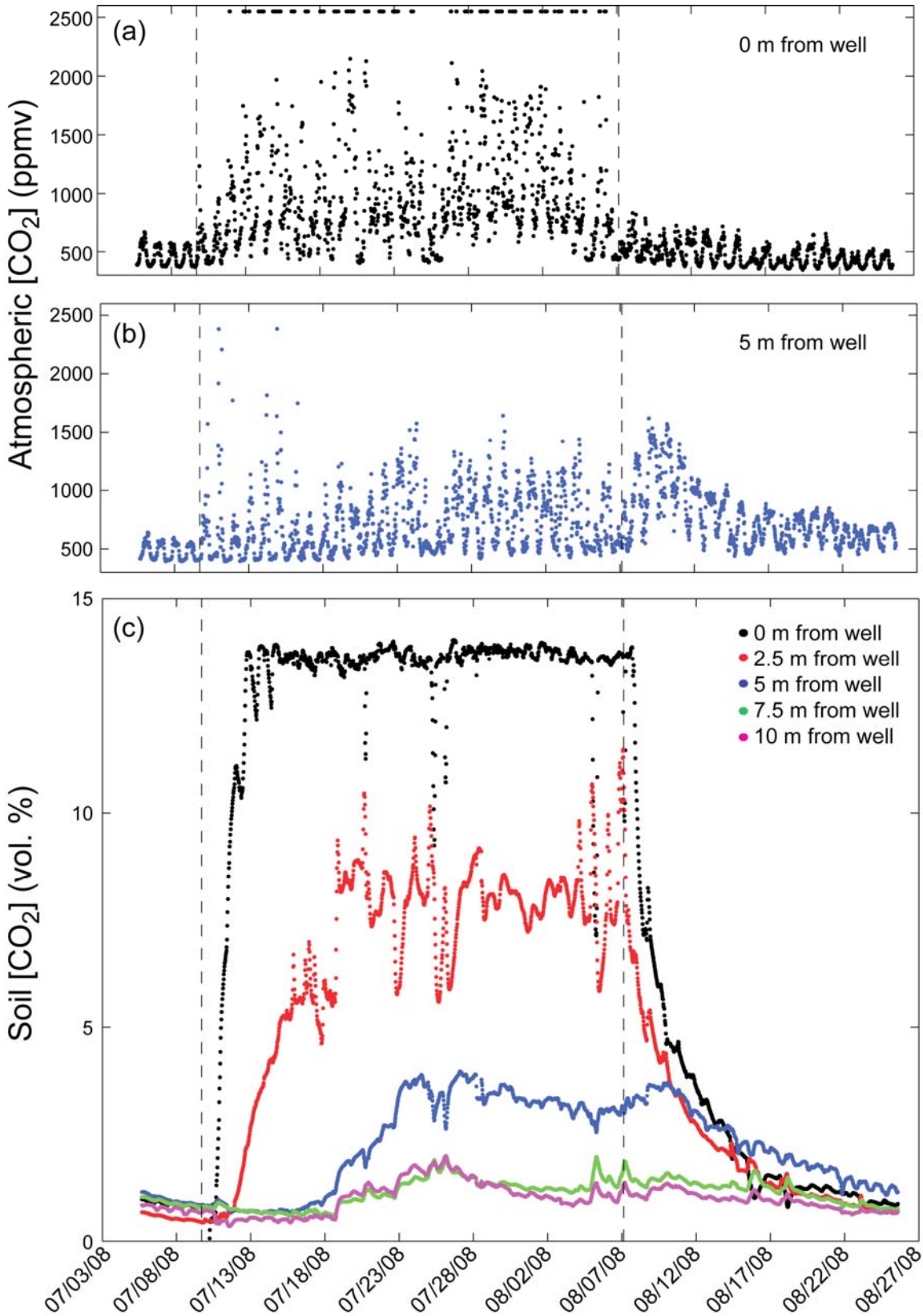
(a)
0 m from well
(b)
5 m from well
(c)
0 m from well
2.5 m from well
5 m from well
7.5 m from well
10 m from well
Atmospheric [CO2] (ppmv)
Soil [CO2] (vol. %)
2500
2000
1500
1000
500
15
10
5
0
07/03/08
07/08/08
07/13/08
07/18/08
07/23/08
07/28/08
08/02/08
08/07/08
08/12/08
08/17/08
08/22/08
08/27/08

Figure 6.

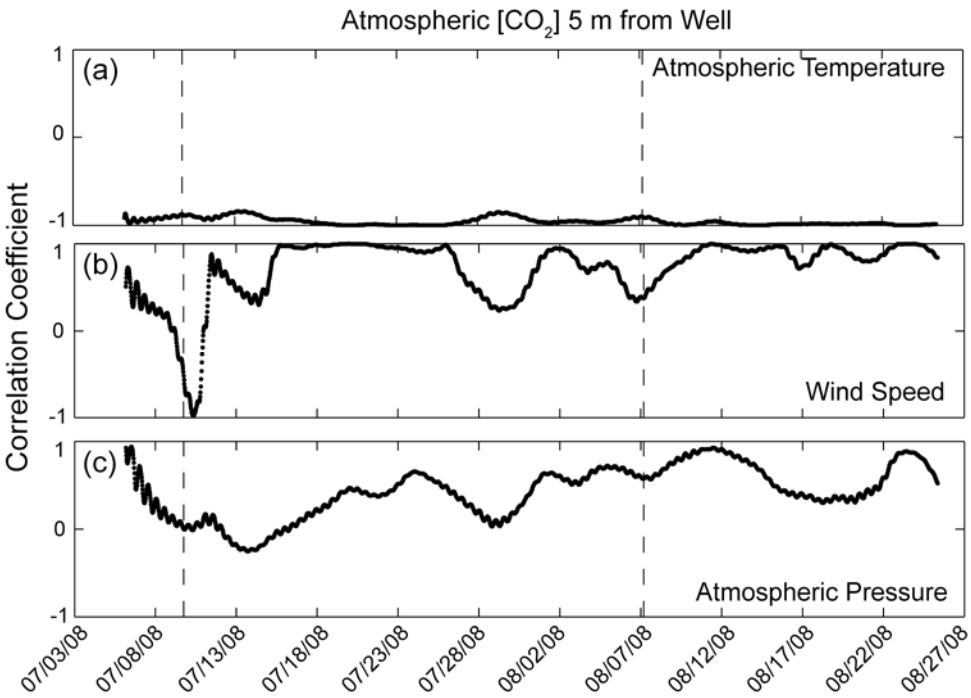

Figure 7.

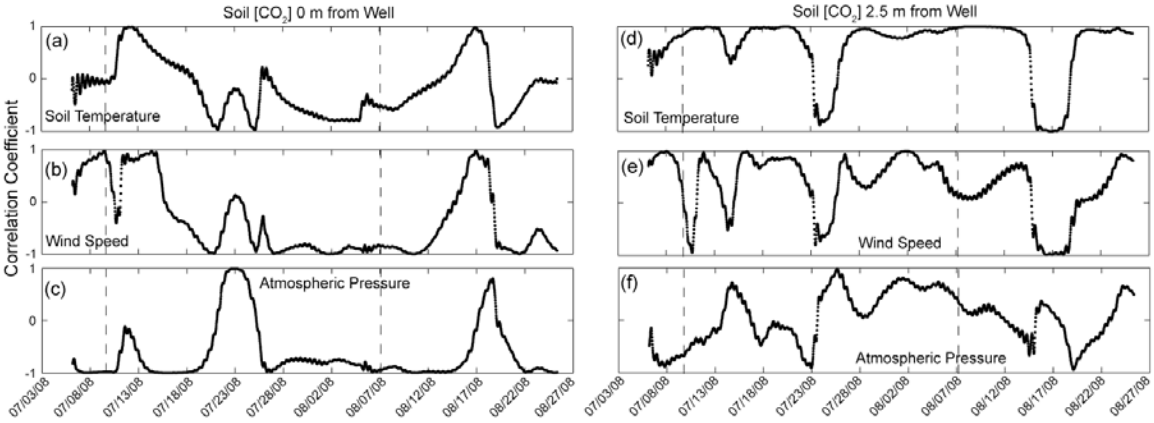

Figure 8.

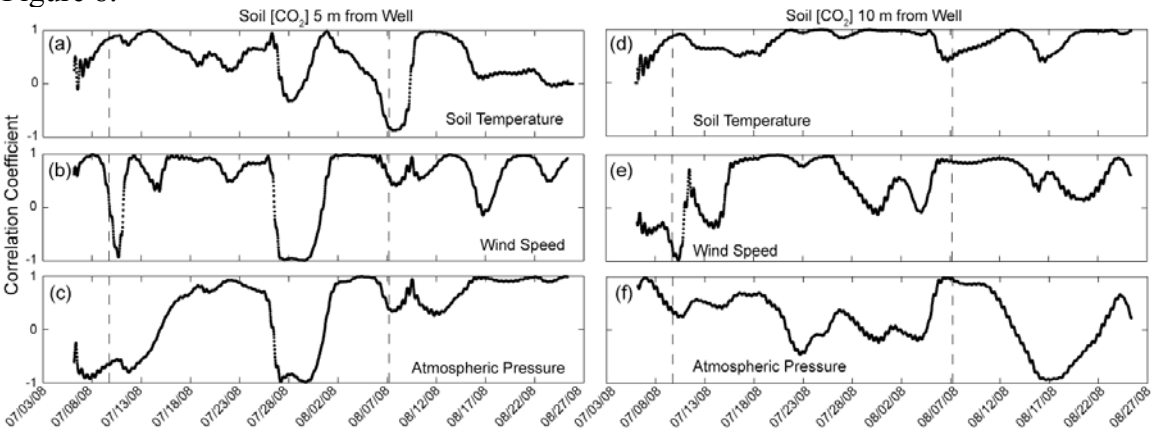

Figure 9.

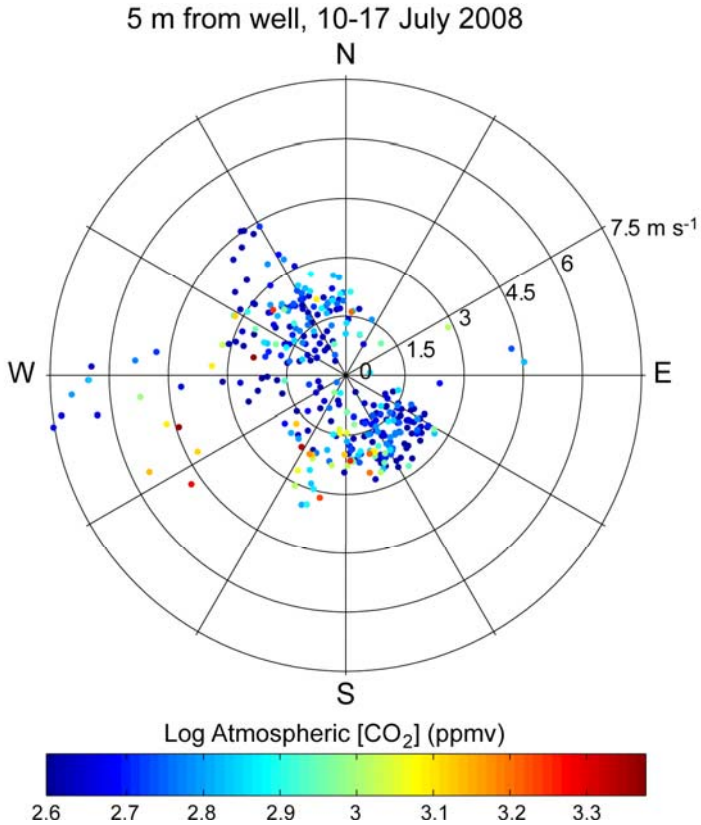
5 m from well, 10-17 July 2008
N
S
W
E
7.5 m s-1
6
4.5
3
1.5
0
Log Atmospheric [CO2] (ppmv)
2.6
2.7
2.8
2.9
3
3.1
3.2
3.3
Figure 10.